JOURNAL OF MAGNETIC RESONANCE, Series B 104, 1–10 (1994)

# WET, a $T_1$- and $B_1$-Insensitive Water-Suppression Method for *in Vivo* Localized $^1$H NMR Spectroscopy

ROBERT J. OGG, PETER B. KINGSLEY, AND JUNE S. TAYLOR

*Department of Diagnostic Imaging, St. Jude Children's Research Hospital, 332 North Lauderdale, Memphis, Tennessee 38101*

Received January 11, 1993; revised July 22, 1993

**Suppression of the water signal during $^1$H magnetic resonance spectroscopy by repeated sequences of a frequency-selective radiofrequency pulse and a gradient dephasing pulse requires nulling of the longitudinal component of the water magnetization and is therefore affected by $T_1$ relaxation, RF-pulse flip angles (which depend on $B_1$), and sequence timing. In *in vivo* applications, $T_1$ and $B_1$ inhomogeneity within the sample may cause spatially inhomogeneous water suppression. An improved water-suppression technique called WET (*w*ater suppression *e*nhanced through $T_1$ effects), developed from a Bloch equation analysis of the longitudinal magnetization over the $T_1$ and $B_1$ ranges of interest, achieves $T_1$- and $B_1$-insensitive suppression with four RF pulses, each having a numerically optimized flip angle. Once flip angles have been optimized for a given sequence, time-consuming flip-angle adjustments during clinical examinations are eliminated. This water-suppression technique was characterized with respect to $T_1$ variations, $B_1$ variations, off-resonance effects, and partial saturation effects and was compared to similar techniques. Effective water suppression has been achieved with this new technique in single-voxel spectroscopy examinations of more than 50 brain tumor patients at 1.5 T.** 

## INTRODUCTION

Selective water excitation followed by gradient dephasing (*1–5*) is a commonly used method for water suppression in the single-scan localization methods for magnetic resonance spectroscopy implemented on clinical instruments, STEAM (90°—TE/2—90°—TM—90°—TE/2—Acquire) (*6*) and PRESS (90°—$TE_1$—180°—$TE_{1+2}$—180°—$TE_2$—Acquire) (*7*). A single water-suppression (WS) sequence consists of a frequency-selective radiofrequency excitation pulse followed by a delay period containing a gradient dephasing pulse (Fig. 1) and suppresses the water signal by randomizing the water magnetization at some time during the MRS sequence. Typically the WS sequence is repeated to improve the water suppression. Water-suppression sequences are placed in the preparation period (TP) before the localization sequence, and sometimes in the TM period in STEAM (*3, 4*).

For WS sequences in TP, effective water suppression requires complete dephasing of the transverse water magnetization and nulling of the longitudinal water magnetization at the time of the first RF pulse in the localization sequence. Moonen and co-workers have analyzed the requirements for dephasing and prescribe a method to avoid producing water signal echoes due to the repeated water-suppression RF pulses (*4, 8*). Nulling the longitudinal water magnetization requires a fixed relationship among the RF flip angles, the interpulse delays, and the range of $T_1$ in the volume element (voxel) of interest. In contrast, for WS sequences during the TM period in STEAM spectroscopy, longitudinal relaxation may be neglected because $T_1$ relaxation during TM leads to signal loss in the stimulated echo signal from the voxel.

Two basic schemes for water suppression in TP have been implemented in practice. Throughout this paper, different *arrangements of repeated WS sequences* will be called *WS methods*. The *n*-pulse equal-angle methods use RF pulses (usually three) with equal flip angles and with equal delay periods long enough to accommodate the gradient dephasing pulses (*4, 8*). The RF pulse flip angle must be adjusted for each voxel to compensate for $T_1$ and $B_1$ effects. The *n*-pulse inversion-recovery methods utilize 180° pulses (usually two) with variable delay times which must be adjusted for each voxel (*9, 10*). [These methods should not be confused with WEFT, in which a nonselective 180° pulse is applied and the water signal is eliminated by differential $T_1$ relaxation (*11*).] Both approaches achieve suppression by adjusting the WS sequence parameters to minimize the net water magnetization. In any region of interest, the residual water signal represents the sum of components with different $T_1$ and perhaps subject to different $B_1$. In single-voxel experiments, good suppression can be achieved, but the WS must be adjusted for each region of interest. In 2D and 3D chemical-shift imaging (CSI) experiments, intervoxel $T_1$ and $B_1$ inhomogeneity can lead to spatial inhomogeneity in suppression (*8*). We demonstrate that suppression with repeated WS sequences can be made essentially independent of $T_1$ and $B_1$ (over relevant ranges of these parameters for *in vivo* spec-



1064-1866/94 $6.00

troscopy with volume coils) by the appropriate choice of the flip angles for each of the RF pulses. These will be called *n*-pulse variable-angle, or WET (*w*ater suppression *e*nhanced through $T_1$ effects), methods.

This paper describes the optimization of the flip angles for the WET WS method, characterizes the behavior of this new method with respect to $T_1$, $B_1$, off-resonance effects, and partial saturation, and demonstrates the effectiveness of the variable-angle WS method in clinical $^1$H MRS. Water-suppression sequences during the TM period in STEAM are also analyzed, and phantom and *in vivo* results demonstrate their behavior.

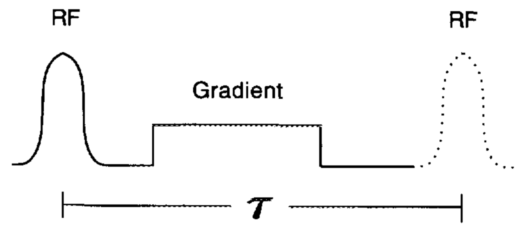


FIG. 1. Diagram of a single water-suppression sequence, consisting of a frequency-selective RF pulse followed by a dephasing gradient pulse. The interpulse delay, $\tau$, is measured from pulse center to pulse center between successive water-suppression sequences or between the water-suppression pulse and the next pulse of the localization sequence.

## THEORY

Following a single WS sequence of length $\tau$ with flip angle $\theta$ (Fig. 1), neglecting the finite width of the RF pulse, the residual longitudinal water magnetization, $M_R$, is

$$M_R = M_I e^{-\tau/T_1}\cos\theta + M_0(1 - e^{-\tau/T_1}), \qquad [1]$$

where $M_0$ is the equilibrium magnetization and $M_I$ is the magnetization at the beginning of the sequence. With *n* WS sequences, the *n* RF flip angles ($\theta_i$) and *n* delay times ($\tau_i$) may be adjusted to achieve the desired $B_1$ and $T_1$ insensitivity of water suppression. We fixed the delay times at 60 ms, the shortest time needed on our system to accommodate the RF pulses, gradient dephasing pulses, and eddy-current-decay periods. Fixing the delay intervals at the shortest practical value improved $T_1$ insensitivity and minimized the total time required for water suppression.

For *n* WS sequences with equal $\tau$, neglecting the finite width of the RF pulses and assuming complete dephasing (*4, 8*) between RF pulses, the residual water magnetization is

$$\begin{aligned} M_R(n) = {} & M_I e^{-n(\tau/T_1)}\cos\theta_1\cos\theta_2\cdots\cos\theta_n \\ & + M_0(1 - e^{-\tau/T_1})[e^{-(n-1)(\tau/T_1)}\cos\theta_2 \\ & \cdots\cos\theta_n + \cdots + e^{-\tau/T_1}\cos\theta_n + 1], \qquad [2] \end{aligned}$$

where $M_I$ is the longitudinal magnetization at the beginning of the *n* water suppression sequences, and $\theta_i$ is the flip angle of the *i*th RF pulse. Throughout this paper, $M_R$ and $M_I$ will be expressed in units of $M_0$, unless otherwise noted.

The gradients and RF-pulse phases of the localization sequence are designed to select a specific coherence pathway: in STEAM, $p = (1, 0, -1)$, and in PRESS, $p = (-1, 1, -1)$ (*12*). With STEAM or PRESS, longitudinal water magnetization in the voxel at the time of the first localization pulse will be refocused at the time of the echo. For WS sequences in TP, parameters must be selected to null accurately water magnetization in the voxel ($M_R = 0$ in Eq. [2]). In the variable-angle method, WS flip angles are selected by numerical optimization of Eq. [2] to minimize $M_R$ over a range of $T_1$ and $B_1$. Spins that undergo $T_1$ relaxation after the first localization pulse and dephasing gradient lose any phase information they had acquired, so their effective coherence level up to that point is 0. Thus, the signal from intravoxel water that relaxes after the first localization pulse and from water outside the voxel will be attenuated by the localization procedure because these components of magnetization will not follow the selected coherence pathway. The signal from intravoxel water that was not suppressed during TP can be reduced by WS sequences in TM. For WS sequences in TM, the optimal RF flip angle is 90° because $T_1$ relaxation after the first localization pulse, including between WS RF pulses in TM, leads to signal loss in the stimulated echo (effective $T_1 = \infty$ in Eq. [2]).

## MATERIALS AND METHODS

*Calculations.* Numerical optimization of variable-angle WS sequences was performed on a personal computer (IBM PC compatible). The RF flip angles were optimized for $400 \leq T_1 \leq 2000$ ms and $B_1$ within ±10% of the nominal value. This covers the range of *in vivo* water $T_1$ values in normal and pathological brain tissue at 1.5 T (*13*) and the expected $B_1$ variation over the brain in a typical quadrature head coil. The flip angles were optimized by a quasi-Newton method (*14*) to minimize $|M_R|$ when $T_1$, $B_1$, or both $T_1$ and $B_1$ were varied, as follows. An array of $M_R$ values was calculated from Eq. [2] either for $400 \leq T_1 \leq 2000$ ms in steps of 200 ms or for $B_1$ within ±10% of the nominal value in steps of 2%, or for both these ranges of parameters. The $\theta_i$ were then adjusted to maintain the absolute value of all members of the array of $M_R$ values below some threshold. The solution was further constrained to maintain the $M_R$ values for $T_1 =$ 800 ms (typical brain parenchyma) and nominal $B_1$ below a lower threshold. This additional constraint was included to force the solution toward better performance at the most common $T_1$ and $B_1$. For a given *n*, the angles were adjusted as the $M_R$ threshold was decreased until no further improvement could be made. Flip angles were constrained to be $\leqslant 180°$ to avoid suboptimal solutions with angles near 270°.

$M_I$ was included in the calculations as a function of $T_1$ and the overall TR of the spectroscopy sequence:

$$M_I = M_0(1 - e^{-TR/T_1}). \quad [3]$$

In a localized spectroscopy sequence, the partial saturation of water magnetization is more complicated than this model because water in different spatial regions is saturated to different degrees by the combination of water-suppression pulses and spatially selective pulses. However, simulations and phantom measurements show that the optimized water suppression is fairly insensitive to $M_I$ for the range of TR/$T_1$ encountered in localized spectroscopy at 1.5 T.

Off-resonance effects were calculated from Eq. [2]. The effective pulse flip angle (away from the $z$ axis) at a given frequency offset ($-100 \leqslant \Delta f \leqslant 100$ Hz) was calculated by numerical integration of the Bloch equations. A separate solution was calculated for each on-resonance flip angle because the magnetization dynamics are nonlinear with respect to RF pulses (*15*). The Bloch equations were integrated using the Bulirsch–Stoer method (*14*).

*NMR measurements.* All measurements were made on a Siemens 1.5 T Magnetom SP (Siemens Medical Systems, Iselin, New Jersey) with the standard quadrature head coil and STEAM localization for $^1$H MR spectroscopy. A two-step 0°/180° phase cycle of the first and third 90° RF pulses was used to eliminate the residual out-of-voxel signal from the third pulse. For WS in TP, TE/TM = 20/30 and 270/30 ms, and for WS in TM, TE/TM = 20/135 ms. TR was 3000 ms. The water-suppression RF pulses were Gaussian-modulated and 25.6 ms in duration, with $\tau$ = 60 ms unless otherwise noted. The bandwidth of a single WS RF pulse was measured from the residual longitudinal magnetization (full width at half-maximum), and was 60 Hz unless otherwise noted. The gradient-pulse integrals ($G_{\alpha,\beta}$ in ms mT/m, $\alpha = x$, $y$ or $z$, $\beta$ = period in sequence) were as follows. For WS sequences in TP, $G_{x,\tau 1} = G_{y,\tau 1} = G_{z,\tau 1} = G_{z,\tau 2} = G_{y,\tau 3} = -36$, $G_{x,\tau 4} = 73$. For WS sequences in TM, $G_{y,\tau 1} = G_{x,\tau 2} = -78$. For STEAM with TE/TM = 270/30 ms, $G_{z,TE/2} = 34$, $G_{y,TM} = 51$, $G_{z,TM} = 100$. For STEAM with TE/TM = 20/30 ms, $G_{x,TE/2} = G_{z,TE/2} = 11$, $G_{y,TE/2} = 12$, $G_{y,TM} = 51$, $G_{z,TM} = 100$. For STEAM with TE/TM = 20/135 ms, $G_{x,TE/2} = G_{y,TE/2} = G_{z,TE/2} = 6$, $G_{y,TM} = 49$, $G_{z,TM} = 52$.

Spectroscopy voxels ($2^3$ ml, unless otherwise noted) were selected from MR images through the region of interest. Localized shimming was performed over each voxel by adjustment of the linear corrections. Signals were sampled at 2048 points over a spectral width of 2000 Hz. The magnitude of the residual water magnetization, $|M_R|$, was calculated from TE = 20 ms measurements as the peak signal intensity in the water line region ($\approx$4.7 ± 0.3 ppm) of the water-suppressed magnitude spectrum divided by the peak height of the water line in the unsuppressed magnitude spectrum.

*In vitro* samples (phantoms) included an 11.5 ml sphere filled with tap water ($T_1 \approx 2500$ ms), a 3 liter sphere filled with $NiSO_4$-doped water ($T_1 \approx 300$ ms), a set of five 15 ml spheres filled with $NiCl_2$-doped water ([$NiCl_2$] = 1.6, 0.8, 0.4, 0.2, 0.0 g/liter, $T_1 \approx$ 200, 400, 800, 1200, 3000 ms), a 1 liter sphere filled with distilled water, and a set of three 166 ml (5.5 cm side) cubic volumes filled with $NiCl_2$-doped water ($T_1 \approx$ 400, 800, 1200 ms) placed in a cylindrical bath (7 cm radius, 6 cm height) of 0.9% NaCl solution (Fig. 2). $T_1$ values for phantoms were estimated by progressive saturation (*16*). *In vivo* measurements included STEAM-localized single-voxel brain spectra in a volunteer and more than 50 pediatric oncology patients, including a series of 32 successive patients examined with a fixed protocol. Informed consent was obtained for all subjects prior to spectroscopy examinations.

## SIMULATION RESULTS

*Effects of varying $T_1$ on $M_R$.* Figure 3a shows $M_R$ versus $T_1$ for the two-, three-, and four-pulse variable-angle WS methods with nominal $B_1$ and on-resonance RF pulses. Also

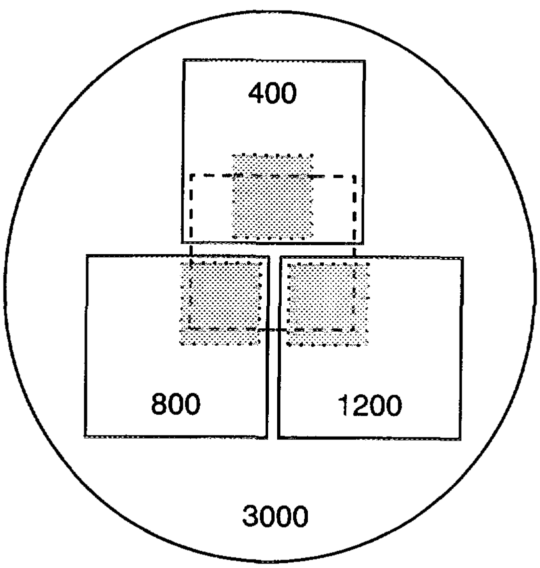


FIG. 2. A phantom used to test $B_1$ and $T_1$ insensitivity of water-suppression methods. The outer circle represents a cylindrical bath (radius = 7 cm, height = 6 cm) containing a 0.9% NaCl solution with $T_1 \approx 3000$ ms. The square regions with solid borders represent 166 ml cubic volumes of $NiCl_2$ solutions with $T_1 \approx$ 400, 800, or 1200 ms, as labeled. The large square with the dashed border indicates the 4 × 2 × 4 cm$^3$ voxel selected to encompass all $T_1$ compartments in the sample. The small, shaded squares represent 2 × 2 × 2 cm$^3$ voxels selected within individual $T_1$ compartments.

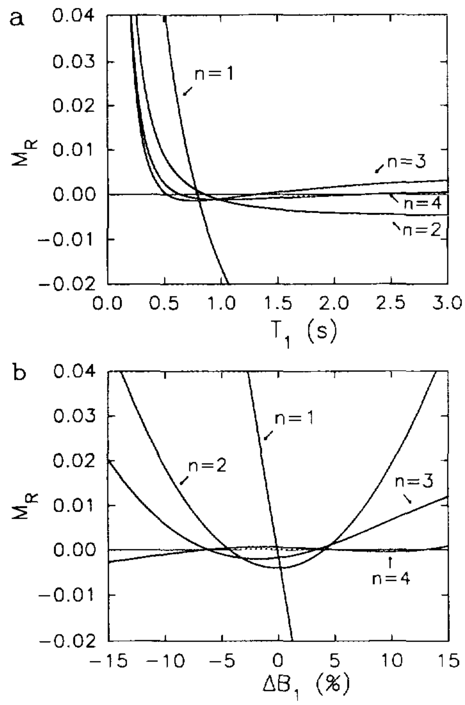


FIG. 3. Effects of varying $T_1$ and $B_1$ separately on $M_R$. (a) Residual water magnetization, $M_R$, versus $T_1$ (nominal $B_1$) following the $n$-pulse variable-angle water-suppression methods, with flip angles chosen to maximize $T_1$ insensitivity. (b) Residual water magnetization, $M_R$, versus $\Delta B_1$ ($T_1$ = 800 ms) following the $n$-pulse variable-angle water-suppression method, with flip angles chosen to maximize $B_1$ insensitivity.

shown for reference is the curve for $n = 1$ with $\theta$ adjusted to null water with $T_1$ = 800 ms ($\theta = 94°$). The pulse angles, optimized with respect to $T_1$ in the range 400–2000 ms, are shown in Table 1. The insensitivity to $T_1$ over the chosen range improved with increasing $n$. The physical basis of the $T_1$ insensitivity can be understood most easily in the two-pulse case, where the optimal angles were ~90° and 180°. Following the 90° pulse, the longitudinal components of the water magnetization evolve with different $T_1$ during the $\tau$ period. After the 180° pulse, the longitudinal components are inverted and begin to "refocus." The refocusing is not perfect because $T_1$ relaxation is nonlinear, and it fails for components with very short $T_1$.

*Effects of varying $B_1$ on $M_R$.* Figure 3b shows $M_R$ versus $\Delta B_1$ for the two-, three-, and four-pulse variable-angle WS methods with $T_1$ = 800 ms and on-resonance RF pulses. Also shown for reference is the curve for $n = 1$ with $\theta = 94°$. The pulse angles, optimized for $\Delta B_1$ in the range of ±10%, are shown in Table 1. The $B_1$ insensitivity of suppression improved with increasing $n$. The basis of the $B_1$ insensitivity is similar to that described above for $T_1$ insensitivity. At a given $T_1$, different values of $B_1$ give different longitudinal magnetizations which then evolve toward equilibrium. With arbitrary $\tau$, $B_1$ insensitivity is maximized for $\theta = 180°$ because dispersion of the longitudinal components of magnetization is minimized for a given range of $B_1$. The use of 180° pulses requires relatively long $\tau$ periods to allow the longitudinal magnetization to relax to the required null. For the relatively short $\tau$ = 60 ms chosen here, optimal $B_1$ insensitivity was achieved with initial pulses between 75° and 100°, which reduce the magnitude of all longitudinal components. These pulses produce positive residual longitudinal components which are inverted by a final pulse greater than 110° to allow refocusing near the null.

*Effects of varying $T_1$ and $B_1$ on $M_R$.* Because the physical bases of the $T_1$ and $B_1$ insensitivities are similar, a solution which minimizes the sensitivity of the water suppression to both $T_1$ and $B_1$ can be found. The optimal angles for the $n$-pulse variable-angle WS methods are shown in Table 1. No clear relationship was apparent between the $\theta_i$ optimized for simultaneous $B_1$ and $T_1$ insensitivity and the $\theta_i$ optimized for separate $T_1$ and $B_1$ insensitivity. The insensitivity improved with increasing $n$, as was true when $\theta_i$ was optimized for separate $T_1$ and $B_1$ insensitivity (data not shown). Figure 4a shows $M_R$ versus $T_1$ at nominal $B_1$ and at nominal $B_1$ ± 10% for $n$ = 4 (solid curves). Also shown for reference are the curves for $n$ = 1, with $\theta = 94°$ at nominal $B_1$ (dashed curves).

*Effects of varying $\tau$ on $\theta_i$ and $M_R$.* Table 2 shows the optimal flip angles and the maximum $M_R$ for the four-pulse variable-angle method at several values of $\tau$. The flip angles were optimized to minimize sensitivity of the suppression to $T_1$ and $B_1$ (Table 1). For $\tau \neq 60$ ms, the optimization

TABLE 1

**Radiofrequency-Pulse Flip Angles (degrees) for $n$-Pulse Variable-Angle WS Methods Optimized with Respect to Variation of $B_1$, $T_1$, or $B_1$ and $T_1$ ($\tau$ = 60 ms)**

| $n$ | $T_1$[a] | $B_1$[b] | $T_1$ and $B_1$[c] |
|---|---|---|---|
| 1 | 94.5[d] | — | — |
| 2 | 89.4 | 79.7 | 85.9 |
| | 180.0 | 110.2 | 124.9 |
| 3 | 92.6 | 75.8 | 89.2 |
| | 76.4 | 70.5 | 83.4 |
| | 180.0 | 118.8 | 160.8 |
| 4 | 86.8 | 98.2 | 81.4 |
| | 115.9 | 80.0 | 101.4 |
| | 70.9 | 75.0 | 69.3 |
| | 180.0 | 152.2 | 161.0 |

[a] $B_1$ = nominal, $400 \leq T_1 \leq 2000$ ms.
[b] $T_1$ = 800 ms, $-10\% \leq \Delta B_1 \leq +10\%$.
[c] $400 \leq T_1 \leq 2000$ ms, $-10\% \leq \Delta B_1 \leq +10\%$.
[d] $T_1$ = 800 ms.

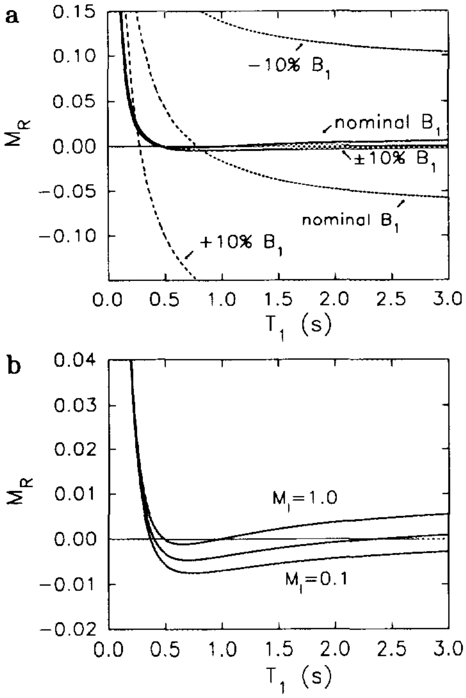


FIG. 4. Effects of varying $B_1$ and $T_1$ simultaneously and of partial saturation on $M_R$. (a) Residual water magnetization, $M_R$, versus $T_1$ following the one-pulse (dashed curves) and four-pulse variable-angle (solid curves) water-suppression methods for nominal $B_1$ and nominal $B_1$ ± 10%. (b) Residual water magnetization, $M_R$, following the four-pulse variable-angle water-suppression method for $M_I$ = 0.1 (bottom curve), 0.5 (middle curve), and 1.0 (top curve).

was begun with the set of flip angles shown for $\tau$ = 60 ms in Table 1. $|M_R|_{max}$ is the magnitude of the maximum residual water magnetization for $-10\% \leq \Delta B_1 \leq 10\%$ and $400 \leq T_1 \leq 2000$ ms. The results in Table 2 show that as $\tau$ decreased, the worst-case suppression over the stated range of $T_1$ and $B_1$ improved, the flip angles of the first and third pulses increased, and the flip angles of the second and fourth pulses decreased. Allowing the delay intervals to vary separately did not further improve water suppression or $B_1$ and $T_1$ insensitivity in simulations.

*Partial saturation effects ($M_I$) on the variable-angle method.* Figure 4b shows $M_R$ versus $T_1$ for $M_I$ = 0.1, 0.5, and 1.0 with the four-pulse variable-angle WS method optimized for $B_1$ and $T_1$ insensitivity. The $T_1$ insensitivity was unchanged and the degree of suppression at a given $T_1$ changed only slightly.

*Off-resonance effects on water suppression.* Figure 5 shows calculated (solid curves) and measured (symbols) values of $M_R$ versus $\Delta f$ for the one-pulse, three-pulse equal-angle, and four-pulse variable-angle WS methods with 60 Hz Gaussian RF pulses. The simulation was calculated with nominal $B_1$ and $T_1$ to model the experimental conditions

TABLE 2

**Effects of Varying the Interpulse Delay, $\tau$, on Water Suppression with the Four-Pulse Variable-Angle Method**

| | $\tau$ (ms) | | | |
|---|---|---|---|---|
| | 40 | 60 | 80 | 100 |
| $\theta_i$ (degrees) | 83.6 | 81.4 | 80.5 | 80.5 |
| | 99.7 | 101.4 | 104.6 | 108.4 |
| | 74.7 | 69.3 | 60.9 | 53.5 |
| | 160.0 | 161.0 | 162.9 | 168.0 |
| $\|M_R\|_{max}$ | 0.003 | 0.005 | 0.008 | 0.009 |

*Note.* RF pulse angles $\theta_i$ (optimized for $-10\% \leq \Delta B_1 \leq 10\%$, $400 \leq T_1 \leq 2000$ ms) and maximum residual water magnetization ($|M_R|_{max}$) following the four-pulse variable-angle WS method for several values of $\tau$ are shown.

under which the data were measured. The variable-angle method used pulse flip angles to minimize $B_1$ and $T_1$ sensitivity and the one-pulse and three-pulse equal-angle methods were adjusted to maximize suppression for $T_1$ = 300 ms. The effective suppression bandwidth (full width at half-maximum suppression) with repeated WS sequences was approximately 50% greater than that with a single WS sequence because of progressive saturation of water magnetization at frequency offsets where the effective $B_1$ is low. The suppression was slightly more uniform for the variable-angle method than for the equal-angle method at frequency offsets less than 30 Hz. We attribute this to the greater $B_1$ insensitivity of the variable-angle method. At frequency offsets greater than 30 Hz, the variable-angle and equal-angle methods gave essentially the same suppression because of the relatively greater ineffectiveness of the 161° Gaussian pulse at these frequency offsets. For example, the effective pulse flip

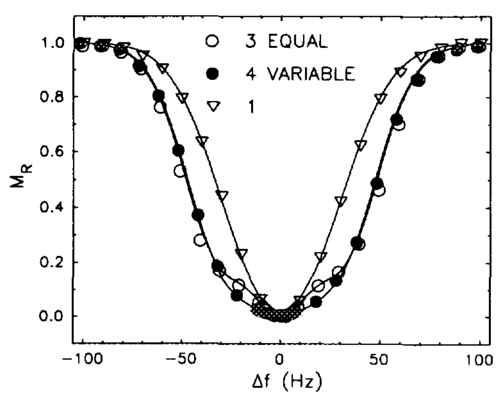


FIG. 5. Off-resonance effects on water suppression. Residual water magnetization, $M_R$, following the one-pulse (open triangles), three-pulse equal-angle (open circles), and four-pulse variable-angle (filled circles) water-suppression methods. The curves were calculated from Eq. [2] as described in the text, and the symbols show measured values.

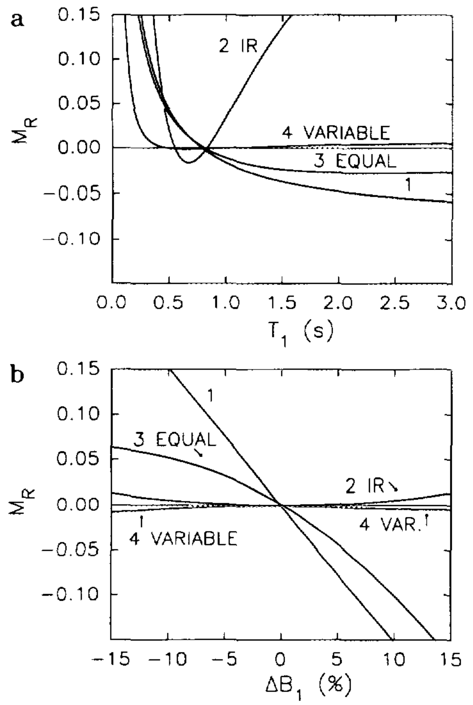


FIG. 6. Comparison of water-suppression methods with respect to $T_1$ and $B_1$ insensitivity. Residual water magnetization, $M_R$, versus (a) $T_1$ and (b) $\Delta B_1$ following the one-pulse, two-pulse inversion-recovery, three-pulse equal-angle, and four-pulse variable-angle water-suppression methods. Except for the variable-angle method, all sequences were calculated to optimize suppression at $T_1$ = 800 ms for nominal $B_1$. The variable-angle method was calculated to optimize $T_1$ and $B_1$ insensitivity (Table 2). The interpulse delay was $\tau$ = 60 ms except in the inversion-recovery method, where a 1 s delay followed the first inversion pulse and the delay following the second pulse was adjusted to optimize suppression at $T_1$ = 800 ms (*9*).

angle (away from the *z* axis) at $\Delta f$ = 40 Hz is 64° for the 161° pulse in the variable-angle method and 59° for the 123° pulses in the equal-angle method. These effective flip angles have cosines of 0.44 and 0.51, respectively. In contrast, at $\Delta f$ = 0, the cosines are −0.95 and −0.55. Therefore, at larger frequency offsets, the residual longitudinal water magnetization is determined by relaxation following repeated low-angle pulses.

*Comparisons with other methods.* The water-suppression methods currently used in proton *in vivo* spectroscopy cannot achieve simultaneous $B_1$- and $T_1$-insensitive water suppression comparable to that of the variable-angle method. Figure 6 shows $M_R$ versus (Fig. 6a) $T_1$ (nominal $B_1$) and (Fig. 6b) $\Delta B_1$ ($T_1$ = 800 ms) for one-pulse, two-pulse inversion-recovery, three-pulse equal-angle, and four-pulse variable-angle WS methods, and on-resonance. Except for the four-pulse variable-angle method, all sequences were adjusted for maximum suppression at $T_1$ = 800 ms. The double-inversion-recovery method had the first delay fixed at 1 s and the second delay was adjusted to optimize suppression (*9*). Equal-angle WS methods gave increased effective suppression bandwidth and slightly improved $T_1$ and $B_1$ insensitivity, relative to a single WS sequence. Our analysis and measurements show that only an odd number of WS sequences should be used in TP when $\theta$ and $\tau$ are equal for all WS sequences because no root exists for Eq. [2] when $n$ is even (*17*). Inversion-recovery WS methods provided good $B_1$ insensitivity, but were very sensitive to $T_1$ because of the long delay intervals needed with the inversion pulses.

A WS method which achieved $T_1$- and $B_1$-insensitive water suppression with adiabatic pulses at 4.7 T has been reported (*18*). Three RF pulses were used with flip angles of 90°, 180°, and 180°. The interpulse delays were selected by analytical solution of an equation similar to Eq. [2], but with variable $\tau$, to give $M_R = 0$ and either $\partial M_R/\partial T_1 = 0$ or $\partial M_R/\partial B_1 = 0$ for a given $T_1$ and nominal $B_1$. With this "hybrid" method (fixed but unequal $\theta_i$, variable delays), the $T_1$ and $B_1$ insensitivities achieved ($|M_R|_{max} = 0.01$, interpulse delays adjusted for $T_1$ = 800 ms) only become comparable to those of the four-pulse variable-angle method ($|M_R|_{max} = 0.005$) when $\theta_1$ in the hybrid method is assumed to be exactly 90° [as in (*18*)]. The $B_1$ insensitivity of WS with the hybrid method is reduced when the flip angle of the first pulse deviates from 90° (data not shown). The four-pulse variable-angle method achieves better $T_1$- and $B_1$-insensitive WS without adiabatic RF pulses in less time (0.24 s) than the hybrid method (~1 s).

## EXPERIMENTAL RESULTS

*Comparison of equal-angle and variable-angle methods.* The variable-angle method was compared experimentally with the commonly used three-pulse equal-angle WS method (*4*). Figure 7 shows measurements of $M_R$ as a function of $T_1$ for the three-pulse equal-angle WS method

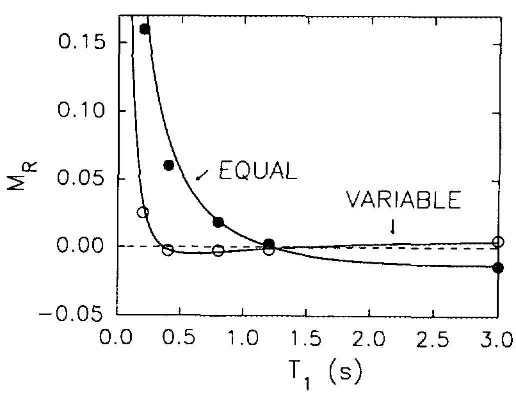


FIG. 7. Water suppression measurements comparing the three-pulse equal-angle (filled circles) and three-pulse variable-angle (open circles) methods with respect to $T_1$ insensitivity. The curves through the measured data were calculated from Eq. [2].

(filled symbols) and the three-pulse variable-angle WS method (open symbols). The measurements were made with the set of five 15 ml spheres described above. First, the sample with $T_1$ = 1200 ms was placed at the center of the coil and shimming was performed. The equal-angle method was adjusted to minimize the residual water signal. With the same sample, the residual water signal was measured using the variable-angle method with the angles calculated to minimize $T_1$ sensitivity (see Table 1). Then each of the other $T_1$ samples was placed in the coil and the measurements were repeated using the same flip angles as had been used for the first sample. In addition, for each $T_1$ sample, the water suppression was optimized for the equal-angle method. The optimal angles for the equal-angle method (data not shown) agreed well with theory (*17*). The curves through the measured data are calculated from Eq. [2]. These data demonstrate the accuracy of the model and the superior $T_1$ insensitivity of variable-angle pulses for a given number of WS sequences. Notice that the curve for variable-angle pulses is almost flat for $T_1 \geqslant 400$ ms. As expected, the suppression begins to fail for shorter values of $T_1$.

Table 3 summarizes measurements of $M_R$ comparing the three-pulse equal-angle and four-pulse variable-angle WS methods with respect to $T_1$ and $B_1$ sensitivity. These measurements were made with the sample diagrammed in Fig. 2. First, a $4 \times 2 \times 4$ cm$^3$ voxel (dashed square in Fig. 2) was selected to include portions of all $T_1$ values present in the sample, analogous to voxel preselection in CSI experiments. Field homogeneity was shimmed over this composite voxel and was not subsequently adjusted for other smaller voxels. The bandwidth of the selective RF pulses in the WS sequences was increased to 240 Hz to compensate for increased water linewidth caused by the phantom structure. The sequence with three equal-angle pulses was adjusted to minimize the residual water signal. With the same voxel, including all $T_1$ values, the residual water magnetization was measured with the variable-angle method using the pulse angles calculated to minimize $B_1$ and $T_1$ sensitivity. Next, $2 \times 2 \times 2$ cm$^3$ cubic voxels (gray-shaded squares in Fig. 2) were selected within each of the compartments containing doped water, overlapping as much as possible with the volume of the larger voxel in that compartment. Residual magnetization was measured with each sequence using the same pulse angles as in the composite voxel. Finally the composite voxel was selected again, and the residual magnetization was measured with the transmitter amplitude for the WS pulses adjusted by ±10% of its nominal value in each of the sequences. The level of suppression was about the same for the two sequences in the composite voxel when the pulse angle of the equal-angle method was optimized. However, the suppression in the individual $T_1$ compartments was much less homogeneous for the equal-angle method, and suppression with the equal-angle method decreased significantly with variation in $B_1$, while it was almost unchanged for the variable-angle method.

**TABLE 3**

**Measurements of $M_R$ in the Phantom Shown in Fig. 2, Comparing the Four-Pulse Variable-Angle and the Three-Pulse Equal-Angle WS Methods with Respect to $B_1$ and $T_1$ Insensitivity**

| $B_1$ (%) | $T_1$ (ms) | $M_R$ Three equal | $M_R$ Four variable |
|---|---|---|---|
| Nominal | Composite[a] | 0.005 | 0.004 |
| Nominal | 400 | 0.017 | 0.004 |
| Nominal | 800 | 0.030 | 0.006 |
| Nominal | 1200 | 0.050 | 0.007 |
| +10 | Composite[a] | 0.104 | 0.004 |
| −10 | Composite[a] | 0.051 | 0.007 |

[a] The composite voxel included regions with $T_1$ = 400, 800, 1200, and 3000 ms as shown in Fig. 2.

*Off-resonance effects on water suppression.* The symbols in Fig. 5 show measurements of $M_R$ versus $\Delta f$ for the one-pulse, the three-pulse equal-angle, and the four-pulse variable-angle methods, in the 3 liter phantom ($T_1$ = 300 ms). The data agree well with the calculated values shown by the solid lines and confirm the increased effective suppression bandwidth with repeated WS sequences.

*Partial saturation effects on water suppression.* $M_R$ was measured as a function of TR for the four-pulse variable-angle WS method in the 1 liter spherical phantom ($T_1$ = 3000 ms). For $1600 \leqslant \mathrm{TR} \leqslant 6000$ ms, $M_R$ was in the range 0.004–0.006, confirming the simulation results showing that partial saturation has little effect on water suppression with the optimized four-pulse variable-angle WS method (Fig. 4b).

*Water-suppression sequences during TM in STEAM.* Water suppression with one or two WS sequences in the TM period (none in TP) of STEAM (TR/TE/TM = 3000/20/135) was measured in the 3 liter phantom and a volunteer. In all measurements, $M_R$ was minimized for $\theta = 90° \pm \sim 1°$. The uncertainty in $\theta$ represents an estimate of the inaccuracy in determining the flip angle in the volume of interest rather than a statistical deviation. Suppression improved with increasing $n$: in the phantom, $M_R$ = 0.011 for $n$ = 1 and 0.001 for $n$ = 2, and in the volunteer, $M_R$ = 0.013 for $n$ = 1 and 0.009 for $n$ = 2. For $n$ = 1 (phantom), the optimal $\theta = 90°$ was unchanged when $\tau$ was increased from 60 ms to 120 ms. These results indicate that water suppression during the TM period is $T_1$-insensitive.

*Clinical results.* The four-pulse variable-angle WS method has been used in clinical spectroscopy examinations of more than 50 pediatric oncology patients. Clinical data were acquired using STEAM localization with TE = 20 and

270 ms in each patient. Measurements were made in tumor, peritumoral, and uninvolved (control) tissues located in various regions of the brain, including all cerebral lobes, thalamus, optic pathway, cerebellum, and pons. Several patients were examined after contrast-enhanced (Gd-DTPA) imaging.

Figure 8 shows $|M_R|$, at TE = 20 ms, from a series of 32 successive patients (65 voxels in 47 examinations), examined under a fixed protocol and *without adjustment* of the water-suppression RF pulses: mean = 0.0027, median = 0.0019, and standard deviation = 0.0027. Excluding the two voxels in which $|M_R| > 0.01$, mean = 0.0023, median = 0.0018, and standard deviation = 0.0015. Water suppression was effective after contrast-enhanced imaging, even in voxels within enhancing tissues. Figure 9 shows representative water-suppressed proton spectra from a voxel in a cystic tumor in the right thalamus and from a control voxel in the left thalamus of a 17-year-old male.

Prior to this series, patients were examined with several modified (STEAM dephasing gradients, phase cycles, WS pulse bandwidth, $B_1$ calibration) spectroscopy sequences. Adequate water suppression was achieved without adjustment of the WS pulses. In some cases in which $|M_R| > 0.005$, two- to fourfold improvements were achieved during the examination by adjusting the flip angle of the final WS pulse or by adjusting the amplitudes of all WS pulses by a common factor. The effectiveness of water suppression was unchanged when the bandwidth of the WS RF pulses was decreased from 60 to 40 Hz.

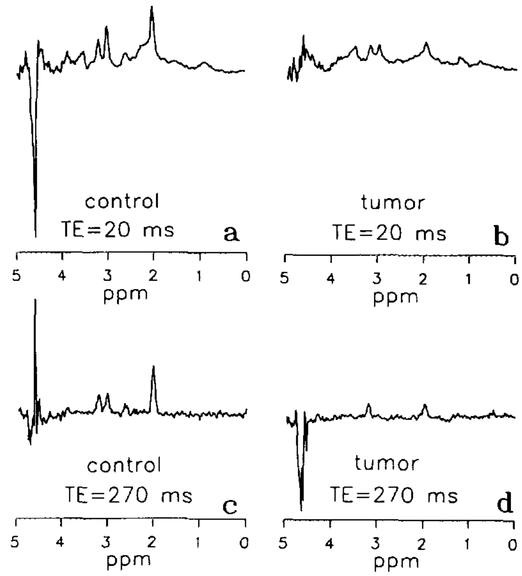


FIG. 9. Water-suppressed *in vivo* proton magnetic resonance spectra from a 17-year-old male with a thalamic tumor. (a) Uninvolved control voxel in the right thalamus, TE = 20 ms. (b) Tumor voxel in the left thalamus, TE = 20 ms. (c) Uninvolved control voxel in the right thalamus, TE = 270 ms. (d) Tumor voxel in the left thalamus, TE = 270 ms. The vertical scale in (c) and (d) is one-half of the vertical scale in (a) and (b). Spectra were acquired with STEAM (TR/TE/TM = 3000/20/30 or 3000/270/30). Water suppression was achieved by the four-pulse variable-angle method with 40 Hz Gaussian RF pulses.

## DISCUSSION

In single-voxel spectroscopy, the primary advantage of the variable-angle WS method is that water suppression can be achieved *without any time-consuming adjustment of the WS RF pulses or interpulse delays.* Eliminating this adjustment reduces the time required to obtain spectroscopy data in clinical examinations and simplifies spectroscopy procedures. In routine clinical application, excellent water suppression has been achieved consistently with the variable-angle method (Figs. 8 and 9).

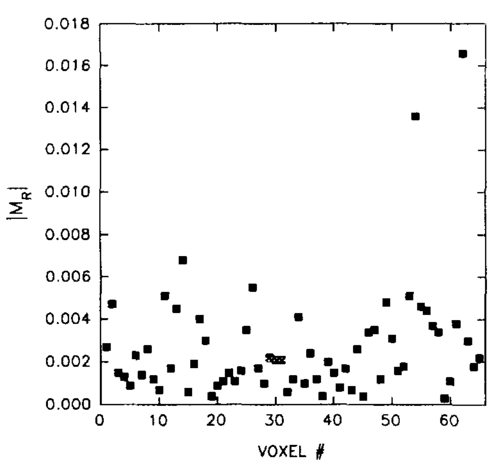


FIG. 8. $|M_R|$ measured in $^1$H brain spectra (TE = 20 ms) from 65 voxels in 47 examinations of 32 pediatric oncology patients.

Three significant points with respect to RF-pulse design for water suppression should be noted. First, the increase in effective suppression bandwidth for repeated WS sequences (Fig. 5) may cause unintended reduction of metabolite signals near the water resonance. The effective bandwidth will depend on the frequency profile and flip angle of the pulses used. Second, the variable-angle method is well suited to the use of crafted RF pulses because the flip angles of the pulses are fixed. This eliminates the need to have sets of crafted RF pulse profiles which maintain the desired frequency profile over a range of on-resonance flip angles (*19*). Third, suppression with the variable-angle method could be improved with adiabatic pulses (*20, 21*) having appropriate bandwidth and range of flip angles, because the resulting $B_1$-insensitive flip angles could be optimized for variation in only $T_1$ (see Fig. 3a).

With the variable-angle WS method, it is important to calibrate the RF system to assure accurate nominal flip angles of the WS RF pulses at the center of the $B_1$ distribution. This is necessary because there may be a difference between the actual $B_1$ in a localized region of interest and an average $B_1$ estimated from a nonlocalized system calibration. When the sequence is implemented, water suppression should be measured in a volunteer, with the voxel in the approximate center of the expected coil $B_1$ distribution, as the amplitudes of the WS RF pulses are varied *together* over a range of $\approx\pm30\%$ around the nominal value determined by the nonlocalized system calibration. The percentage change in RF-pulse amplitudes at the center of the symmetric distribution of water suppression with respect to changes in $B_1$ should then be used to adjust the flip angles used for the region of interest. For example, we have increased the flip angles specified in the pulse sequence by 8% for brain spectroscopy with the standard quadrature head coil. If improved suppression is desired during single-voxel spectroscopy examinations, the variable-angle method can be optimized for a given voxel by adjusting the flip angle or interpulse delay of the final WS sequence, or the flip angles of all WS pulses by a common factor. During CSI examinations, all WS pulse amplitudes should be adjusted by a common factor in order to preserve $B_1$- and $T_1$-insensitive suppression over the extended region of interest.

The requirements for dephasing transverse magnetization in localized spectroscopy sequences containing repeated WS sequences have been analyzed extensively (*4, 8*). In our implementation, we began with existing STEAM spectroscopy sequences (TE = 20 and 270 ms) and added the WS sequences with the gradients listed above. With WS in TP, we observed small spurious peaks over a range of $\pm0.7$ ppm around the water peak in some measurements, which were eliminated by sequence-specific empirical adjustments to the homogeneity-spoiling gradients in the TM period. The particular sets of gradients chosen for each sequence represent an effective compromise within the constraints of sequence timing and gradient hardware.

The results of our numerical optimization of the RF flip angles for the variable-angle method have provided satisfactory and robust water suppression under the conditions of our single-voxel STEAM clinical spectroscopy examinations at both long and short TE (270 and 20 ms). We did not exhaustively explore the ranges of all parameters affecting the solution, so other solutions may exist. Care should be taken to determine the minimum range of $T_1$ insensitivity required and the $B_1$ inhomogeneity of the RF coil over the region of interest. The value of $\tau$ should be as small as possible, subject to the constraints of the required bandwidth of the RF pulses, the dephasing required, and the hardware available. Good $T_1$- and $B_1$-insensitive water suppression can be achieved only if the flip angles of the RF pulses are optimized for the exact conditions of the intended application.

Water suppression during the TM period of STEAM is insensitive to variations in water $T_1$ because of the magnetization dynamics leading to the stimulated echo. However, increasing the length of TM to accommodate WS sequences leads to increased sensitivity to diffusion and patient motion (*22*) and to $T_1$ signal loss from the metabolites of interest. Further, increasing the number of RF pulses creates additional coherence pathways, which complicates the design of the dephasing gradient sequence. With the $T_1$-insensitive suppression we have demonstrated using the variable-angle method in TP, additional water-suppression sequences in TM have been unnecessary.

In CSI experiments, the variable-angle WS method can significantly reduce the spatial inhomogeneity of water suppression by reducing the sensitivity of the water suppression to variations in $B_1$ and $T_1$. Even with the variable-angle WS method, some spatial inhomogeneity may be observed in CSI due to static magnetic field deviations. However, suppression with the variable-angle method is less sensitive than comparable methods to these deviations because of its flatter suppression profile around $\Delta f = 0$ (Fig. 5). The effect on water suppression will depend on the magnitude of the field deviations and the volume of water involved. Preliminary phantom and *in vivo* CSI measurements with four-pulse variable-angle water suppression have shown significant improvements in the magnitude and spatial homogeneity of water suppression compared with the three-pulse equal-angle method (data not shown).

## CONCLUSION

We have shown that: (i) the optimal RF pulse angle is 90° for water-suppression sequences in the TM period of STEAM, (ii) the effective bandwidth achieved with repeated water-suppression sequences is greater than the nominal bandwidth of the single RF pulse used for water suppression, and (iii) a new approach to water suppression with repeated sequences of selective water excitation and gradient dephasing in the preparation period, called WET, achieves suppression that is essentially independent of $B_1$ and $T_1$ for practical *in vivo* applications using volume RF coils by appropriate selection of the flip angles of the water-suppression RF pulses.

With the WET method, excellent water suppression was demonstrated in single-voxel spectroscopy with no adjustment of the water-suppression RF pulses during the patient examinations. This method may reduce the spatial inhomogeneity of water suppression caused by spatial inhomogeneity of $B_1$ or $T_1$ in multivoxel techniques like 2D and 3D CSI.

## ACKNOWLEDGMENTS

This work was supported by National Cancer Institute Grant CA 49516 (to J.S.T.), Cancer Center Support (CORE) Grant P30CA21765, the American Lebanese and Syrian Associated Charities (ALSAC), and Siemens Medical Systems. We thank James Langston, M.D., Mary Jo Freeman, R.T., and Marilyn Pierce, R.T., for their assistance in conducting clinical spectroscopy examinations.

## REFERENCES

1. R. K. Gupta, *J. Magn. Reson.* **24,** 461 (1976).
2. A. Haase, J. Frahm, W. Hänicke, and D. Matthaei, *Phys. Med. Biol.* **30,** 341 (1985).
3. D. M. Doddrell, G. J. Galloway, W. M. Brooks, J. Field, J. M. Bulsing, M. G. Irving, and H. Baddeley, *J. Magn. Reson.* **70,** 176 (1989).
4. C. T. W. Moonen and P. C. M. van Zijl, *J. Magn. Reson.* **88,** 28 (1990).
5. J. Frahm, T. Michaelis, K. D. Merboldt, H. Bruhn, M. L. Gyngell, and W. Hänicke, *J. Magn. Reson.* **90,** 464 (1990).
6. J. Frahm, K. D. Merboldt, and W. Hänicke, *J. Magn. Reson.* **72,** 502 (1987).
7. P. A. Bottomley, *Ann. N.Y. Acad. Sci.* **508,** 333 (1987).
8. C. T. W. Moonen, G. Sobering, P. C. M. van Zijl, J. Gillen, M. von Kienlin, and A. Bizzi, *J. Magn. Reson.* **98,** 556 (1992).
9. F. Träber, J. Bunke, W. A. Kaiser, G. Layer, U. Müller-Lisse, and M. Reiser, Abstracts of the Society of Magnetic Resonance in Medicine, 11th Annual Meeting, p. 1947, 1992.
10. J. H. Duijn, G. B. Matson, A. A. Maudsley, and M. W. Weiner, *Magn. Reson. Imaging* **10,** 315 (1992).
11. S. L. Patt and B. D. Sykes, *J. Chem. Phys.* **56,** 3182 (1972).
12. G. J. Barker and T. H. Mareci, *J. Magn. Reson.* **83,** 11 (1989).
13. P. A. Bottomley, C. J. Hardy, R. E. Argersinger, and G. Allen-Moore, *Med. Phys.* **14,** 1 (1987).
14. W. H. Press, B. P. Flannery, S. A. Teukolsky, and W. T. Vetterling, "Numerical Recipes in C," Cambridge Univ. Press, New York, 1988.
15. R. R. Ernst, G. Bodenhausen, and A. Wokaun, "Principles of Nuclear Magnetic Resonance in One and Two Dimensions," pp. 123–124, Oxford Univ. Press, New York, 1987.
16. R. Freeman, H. D. Hill, and R. Kaptein, *J. Magn. Reson.* **7,** 82 (1972).
17. R. J. Ogg, P. B. Kingsley, and J. S. Taylor, Abstracts of the Society of Magnetic Resonance in Medicine, 11th Annual Meeting, p. 2134, 1992.
18. J. F. Shen and J. K. Saunders, *Magn. Reson. Med.* **29,** 540 (1993).
19. P. Webb, Abstracts of the Society of Magnetic Resonance in Medicine, 11th Annual Meeting, p. 2131, 1992.
20. K. Uğurbil, M. Garwood, and A. R. Rath, *J. Magn. Reson.* **80,** 448 (1988).
21. J. F. Shen and J. K. Saunders, *J. Magn. Reson.* **95,** 356 (1991).
22. G. J. Barker, T. H. Mareci, and K. N. Scott, *J. Magn. Reson.* **64,** 177 (1985).